Available online at www.sciencedirect.com
ScienceDirect
Journal of Power Sources 172 (2007) 265–277
JOURNAL OF POWER SOURCES
www.elsevier.com/locate/jpowsour

Numerical study of cell performance and local transport phenomena in PEM fuel cells with various flow channel area ratios

Xiao-Dong Wang [a], Yuan-Yuan Duan [b], Wei-Mon Yan [c,*]

[a] Department of Thermal Engineering, School of Mechanical Engineering, University of Science and Technology Beijing, Beijing 100083, PR China
[b] Key Laboratory of Thermal Science and Power Engineering of MOE, Tsinghua University, Beijing 100084, PR China
[c] Department of Mechatronic Engineering, Huafan University, Shih-Ting 22305, Taiwan

Received 1 June 2007; received in revised form 13 July 2007; accepted 13 July 2007
Available online 19 July 2007

Abstract

Three-dimensional models of proton exchange membrane fuel cells (PEMFCs) with parallel and interdigitated flow channel designs were developed including the effects of liquid water formation on the reactant gas transport. The models were used to investigate the effects of the flow channel area ratio and the cathode flow rate on the cell performance and local transport characteristics. The results reveal that at high operating voltages, the cell performance is independent of the flow channel designs and operating parameters, while at low operating voltages, both significantly affect cell performance. For the parallel flow channel design, as the flow channel area ratio increases the cell performance improves because fuel is transported into the diffusion layer and the catalyst layer mainly by diffusion. A larger flow channel area ratio increases the contact area between the fuel and the diffusion layer, which allows more fuel to directly diffuse into the porous layers to participate in the electrochemical reaction which enhances the reaction rates. For the interdigitated flow channel design, the baffle forces more fuel to enter the cell and participate in the electrochemical reaction, so the flow channel area ratio has less effect. Forced convection not only increases the fuel transport rates but also enhances the liquid water removal, thus interdigitated flow channel design has higher performance than the parallel flow channel design. The optimal performance for the interdigitated flow channel design occurs for a flow channel area ratio of 0.4. The cell performance also improves as the cathode flow rate increases. The effects of the flow channel area ratio and the cathode flow rate on cell performance are analyzed based on the local current densities, oxygen flow rates and liquid water concentrations inside the cell.

Keywords: Proton exchange membrane fuel cells; Flow channel area ratio; Parallel flow channel design; Interdigitated flow channel design; Electrochemical reaction

1. Introduction

Fuel cells are electrochemical devices that can realize direct conversion of the chemical energy in the reactants to electrical energy with high efficiency and high environment compatibility. A proton exchange membrane (PEM) fuel cell operates at significantly lower temperature than other types of fuel cells, and has received much attention in the past decade due to its many promising applications in portable power sources, automobile power systems, and stationary power plants.

The cell performance of PEM fuel cells depends strongly on the operating conditions, transport phenomena in the cells, electrochemical reaction kinetics, mechanical design, manufacturing process, etc. A number of numerical and experimental investigations have been carried out to understand the transport phenomena and the cell performance of PEM fuel cells. The pioneering work was by Bernardi and Verbrugge [1], who developed a one-dimensional isothermal model to examine the mass transport in fuel cells. Springer et al. [2] proposed an isothermal, one-dimensional model in which the water diffusion coefficient, electro-osmotic drag coefficient, water sorption isotherms, and membrane conductivities were assumed to be functions of the membrane water content. Gurau et al. [3] developed a one-dimensional mathematical model to examine the characteristics of the mass transport of the reactant gas in a half-cell, in which the effects of the porosity and the tortuosity of the gas-diffusion layer and the catalyst layer were explored. Djilali and Lu [4] presented a one-dimensional, non-isothermal model to examine the effects of temperature and gas pressure gradients on fuel cell performance and water management. The first quasi-

* Corresponding author. Tel.: +886 2 2663 2102; fax: +886 2 2663 1119.
E-mail address: wmyan@huafan.hfu.edu.tw (W.-M. Yan).

0378-7753/$ – see front matter © 2007 Elsevier B.V. All rights reserved.
doi:10.1016/j.jpowsour.2007.07.026

Nomenclature

a	chemical activity of water vapor
$Aj_{0,a}^{ref}$	exchange current density at anode (A m^{-3})
$Aj_{0,c}^{ref}$	exchange current density at cathode (A m^{-3})
A_r	flow channel area ratio
b	source term of variable ϕ
C	mass fraction
C_F	quadratic drag factor
d_{porous}	equivalent surface diameter of porous media (m)
D	mass diffusivity (m^2 s^{-1})
$D_{k,eff}$	effective mass diffusivity for the kth species (m^2 s^{-1})
F	Faraday constant (96,487 C mol^{-1})
i	current density (A m^{-2})
I	average current density in the fuel cell (A m^{-2})
I_y	local current density in the y direction (A m^{-2})
j_a	current density at anode (A m^{-3})
j_c	current density at cathode (A m^{-3})
k_c	coefficient of water vapor condensation rate (s^{-1})
k_e	coefficient of water vapor evaporation rate (s^{-1})
k_p	permeability (m^2)
L_c	channel width (m)
L_r	rib width (m)
M	molecular weight (kg mol^{-1})
P	pressure (atm)
P_{sat}	saturated water vapor pressure (atm)
Power	power (W m^{-2})
P'	perturbed variation of pressure in a control volume
R	universal gas constant (8.314 J mol^{-1} K^{-1})
s	volume ratio occupied by liquid water
S'	surface area (m^2)
S_c	corrected source term in the concentration equation
S_j	source term in the phase potential equation
S_L	source term accounting for the liquid water effect
S_u	source term in the x momentum equation
S_v	source term in the y momentum equation
S_w	source term in the z momentum equation
t	time (s)
T	temperature (K)
u	x direction velocity (m s^{-1})
v	y direction velocity (m s^{-1})
V'	volume (m^3)
V_{cell}	operating voltage (V)
w	z direction velocity (m s^{-1})
x	x direction coordinate (m)
y	y direction coordinate (m)
z	z direction coordinates (m)
Z_f	species valence

Greek

α_a	electrical transfer coefficient in forward reaction
α_c	electrical transfer coefficient in backward reaction
ε	porosity
ε_{eff}	effective porosity
ϕ	dependent variables
Φ	phase potential function
η	overpotential (V)
λ	water content in membrane
ν	kinematic viscosity (m^2 s^{-1})
ρ	density (kg m^{-3})
σ_m	electric conductivity of membrane
τ	tortuosity of the pores in the porous medium
Ξ_ϕ	exchange coefficient

superscripts

ref	reference value

subscripts

a	anode
c	cathode
channel	channel
CL	catalyst layer
eff	effective
GDL	gas-diffusion layer
H^+	hydrogen ion
H_2	hydrogen
H_2O	water
k	kth species of the mixture
porous	porous medium
Mem	membrane
O_2	oxygen
sat	saturation
total	total
x	x direction
y	y direction
z	z direction

two-dimensional, along-the-channel model of a PEM fuel cell was established by Fuller and Newman [5] with the assumption of a constant diffusivity of water in the membrane to study water and thermal management issues. Bussel et al. [6] divided a MEA into more than 10 units in a two-dimensional dynamic model to study the water formation, electro-osmosis and diffusion in the PEM, and their effects on cell performance for various operating conditions. Singh et al. [7] employed a two-dimensional model to investigate the transport phenomena in a PEMFC. In their work, the attention was focused on the transport processes in the fuel cells to improve the thermal and water management, and to alleviate the mass transport limitations. Yi and Nguyen [8,9] developed a two-dimensional isothermal model for evaluating the effects of various designs and operating parameters on the performance of a PEM fuel cell. Their results showed that humidification of the anode gas is required to enhance the membrane conductivity and the liquid injection and higher humidification temperatures can improve the cell performance by introducing more water into the anode. Also, higher cathode gas pressures help replenish the water loss by electro-osmosis, thereby making the membrane more conductive and

improving cell performance. Hsing and Futerko [10] developed a two-dimensional model coupling the fluid flow, mass transport and electrochemistry in a PEMFC taking into account the variation of the diffusion coefficient of liquid water in the membrane. Ge and Yi [11] developed a two-dimensional model to investigate the effects of operating conditions and membrane thickness on the water transport. Their study considered the change in effective porosity due to the liquid water to simplify the two-phase transport model in the porous layers. Yan et al. [12] developed a two-dimensional model to investigate gas reactant transport for various flow channel width fractions, λ, and GDL porosities ε. They showed that an increase in either λ or ε may lead to better cell performance, and that a relatively low overpotential gives a more uniform current density distribution across the cell width. Dutta et al. [13] used the commercial code FLUENT to study three-dimensional mass transport and fuel concentration variation and their effects on the electrochemical reaction in PEM fuel cells with serpentine flow channels. Mazumder and Cole [14,15] demonstrated the differences between two- and three-dimensional numerical results and employed a simplified model to discuss the effects of liquid water on cell performance. Um and Wang [16,17] developed a three-dimensional model to deal with the effects of oxygen and vapor and fuel transport on the electrochemical reaction in three-dimensional fuel cells with straight channels and interdigitated channels.

Water management is an important issue in fuel cells. Nguyen and White [18] proposed a model for the water and heat management in PEMFC systems, which includes the effect of electro-osmosis, water diffusion, heat transfer from the solid phase to the gas phase, and latent heat as water evaporates and condenses. Voss et al. [19] developed a relatively novel water management technique with anode water removal to modify the water concentration gradient in the proton exchange membrane to augment the back-diffusion of water from the cathode to the anode where the water at the cathode catalyst layer diffuses through the membrane and is removed via the anode reactant gas stream. Okada et al. [20,21] developed a simple model to investigate water transport in the membrane with their computational results indicating that the water concentration profile is influenced by the thickness and humidity of the membrane and the current density in the cell. Wood et al. [22] presented experimental results for the effectiveness of the direct liquid water injection scheme and interdigitated flow field design for improving PEMFC performance. They found that the interdigitated flow field provides higher transport rates of reactants and products to and from the inner catalyst layers. Baschuk and Li [23] presented a mathematical model with variable degrees of water flooding in the PEMFC with consideration of the physical and electrochemical processes occurring in the membrane electrolyte, the cathode catalyst layer, the electrode backing layer and the flow channel. They found that when air was used as the cathode fuel, the flooding phenomena were similar to experimental results for various operating pressures and temperatures. When the cell pressure is increased significantly, water flooding at the electrode becomes serious and leads to a noticeable reduction in the power output.

The flow channel design in bipolar plates is one of the key factors affecting system performance in PEMFCs. Appropriate flow channel design can enhance the reactant gas transport rate in the flow channel and the gas-diffusion layer before it reaches the catalyst layer for the reaction. Many studies have analyzed the effects of the various types of flow channels, such as the serpentine channel, multiple channels in parallel and interdigitated channels, on the cell performance. Nguyen [24] first proposed the interdigitated flow channel design to enhance liquid water transport out of the diffusion layer. This design converts the transport of reactant/product gases to/from the catalyst layers from diffusion to convection. Yi and Nguyen [9] analyzed the effects of various flow channel designs on PEM fuel cell performance, and concluded that the interdigitated design is superior in accelerating the chemical reaction and improving cell performance. West and Fuller [25] studied the effects of the rib spacing of bipolar plates and the thickness of the gas-diffusion electrode on cell performance. They found that the two-dimensional effect only slightly alters the half-cell potential for a given applied current, but significantly influences the water management. Kazim et al. [26] constructed a two-dimensional, steady half-cell model to investigate the superiority of the interdigitated flow field design over conventional designs, especially in terms of the maximum power density. Their theoretical results showed that the limiting current density in a fuel cell with an interdigitated flow field is about three times the current density in a fuel cell with a conventional flow field. Their results also demonstrated that the interdigitated flow field design can double the maximum power density of a PEM fuel cell. Hu et al. [27,28] considered in detail the effects of the interdigitated design on cell performance. Their results showed that, relative to straight flow channels, the interdigitated design on the cathode side increases the oxygen concentration and reduces the liquid water content in the diffusion layer, but the cell performance is worse if the cathode fuel gas is supplied without humidification. Water molecules occur within the membrane due to the electro-osmotic drag caused by the potential gradient and the back-diffusion caused by water concentration gradient across the cell. When these two driving forces are equal the water in the membrane is in equilibrium. He et al. [29] developed a two-phase model to examine water and thermal management in PEM fuel cells with the interdigitated flow field. They found that the interdigitated gas distributors can reduce the mass-transport overpotential and reduce flooding on the cathode side.

Recently, Yan and co-workers [12,30–37] presented a series of experimental and numerical studies analyzing the effects of various flow field designs on the cell performance in PEMFCs. They found that the flow distributor geometry significantly influences cell performance. In addition, they found that a larger channel width fraction gives faster dynamic response as well as better cell performance. An appropriate bipolar plate flow channel design can significantly improve the thermal efficiency and the water management in PEMFC systems. Therefore, the design of optimal flow channels in the bipolar plate is one of the most important issues in PEMFC designs.

This survey has showed that the fuel flow channel design significantly affects the PEMFC performance. The section

geometry and fuel flow channel design influence the reactant gas transport, water management, and fuel utilization efficiency. If the exhaust gas and waste water are not properly removed, the oxygen supply will be restricted, which will cause the cell to overheat and will dry out the fuel cell system. This unfavorable situation will increase the inter-cell resistance and reduce system performance. An appropriate fuel flow channel design will improve reactant gas transport as well as water management. Through a number of investigations have compared PEMFC performance with the conventional parallel flow channel design and the interdigitated flow channel design, the effects of flow channel area ratio (the ratio of the flow channel area to the total reaction area) on the cell performance have not been comprehensively examined. Furthermore, most previous investigations have utilized simplified two-dimensional models or only considered the essential part of the fuel cell in the computational domain to reduce the computational time. The main objective of the present study is to investigate the effects of flow channel area ratio and cathode fuel mass flow rate on the transport of the reactant gas from the flow channels to the gas-diffusion layer, the liquid water distribution, the local current density, and the PEMFC performance with the conventional parallel flow channel design and the interdigitated flow channel design. The following parts will be organized as follows: Section 2 presents a three-dimensional full-cell model including the effects of the liquid water formation on the reactant gas transport. Section 3 presents the numerical solution procedure, independence, and validation of the numerical results. Section 4 describes the effects of the flow channel area ratio and cathode fuel flow rate on the cell performance and analyzes the local transport phenomena. Section 5 presents conclusions.

2. Analysis

A three-dimensional model of the entire fuel cell (as shown in Fig. 1) was developed to analyze the electrochemical reactions and transport phenomena of the reactants and products in the anode catalyst layer, PEM, and cathode catalyst layer where the reaction occurs. In the other regions such as the gas-diffusion layer, no chemical reactions take place. Therefore, the governing equations include mass, momentum, species and electrical potential conservation equations. The model assumes that:

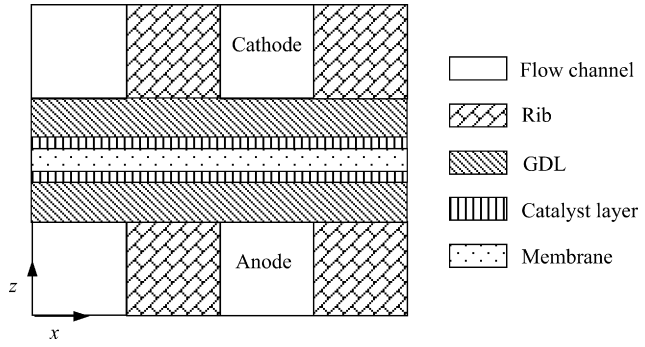

Fig. 1. Schematic of the cross-section of the PEMFC (no scale and only two channels and two ribs are shown).

the system is three-dimensional and steady; the inlet fuels are ideal gas; the system is isothermal; the flow is laminar; the fluid is incompressible; the thermal properties are constant; and the porous layers such as diffusion layer, catalyst layer and PEM are isotropic. With the above assumptions, the gas transport equations for the three-dimensional PEM fuel cell are as follows.

Continuity equation:

$$\frac{\partial u}{\partial x}+\frac{\partial v}{\partial y}+\frac{\partial w}{\partial z}=0 \tag{1}$$

x-Momentum equation:

$$\varepsilon_{\text{eff}}\left(u\frac{\partial u}{\partial x}+v\frac{\partial u}{\partial y}+w\frac{\partial u}{\partial z}\right) = -\frac{\varepsilon_{\text{eff}}}{\rho}\frac{\partial P}{\partial x}+\nu\varepsilon_{\text{eff}}\left(\frac{\partial^2 u}{\partial x^2}+\frac{\partial^2 u}{\partial y^2}+\frac{\partial^2 u}{\partial z^2}\right)+S_u \tag{2}$$

y-Momentum equation:

$$\varepsilon_{\text{eff}}\left(u\frac{\partial v}{\partial x}+v\frac{\partial v}{\partial y}+w\frac{\partial v}{\partial z}\right) = -\frac{\varepsilon_{\text{eff}}}{\rho}\frac{\partial P}{\partial y}+\nu\varepsilon_{\text{eff}}\left(\frac{\partial^2 v}{\partial x^2}+\frac{\partial^2 v}{\partial y^2}+\frac{\partial^2 v}{\partial z^2}\right)+S_v \tag{3}$$

z-Momentum equation:

$$\varepsilon_{\text{eff}}\left(u\frac{\partial w}{\partial x}+v\frac{\partial w}{\partial y}+w\frac{\partial w}{\partial z}\right) = -\frac{\varepsilon_{\text{eff}}}{\rho}\frac{\partial P}{\partial z}+\nu\varepsilon_{\text{eff}}\left(\frac{\partial^2 w}{\partial x^2}+\frac{\partial^2 w}{\partial y^2}+\frac{\partial^2 w}{\partial z^2}\right)+S_w \tag{4}$$

In the momentum equations, S_u, S_v and S_w stand for the source terms based on the Darcy drag forces in the x, y, and z directions imposed by the pore walls on the fluid which usually cause in significant pressure drops across the porous media. The details of S_u, S_v and S_w for different layers are listed in Table 1. In Table 1, ε_{eff} is the effective porosity of the porous material, C_{F} is the quadratic drag factor, and Z_{f} is the ion valence in the PEM. In addition, $D_{k,\text{eff}}$ is the effective diffusion coefficient of the kth species, which was calculated using the Bruggeman equation [29], and k_{p} is the permeability of the porous materials. The relationship between the porosity and the permeability was described by the Blake–Kozeny equation [38],

$$k_{\text{p}}=\left(\frac{d_{\text{porous}}^2}{150}\right)\left[\frac{\varepsilon^3}{(1-\varepsilon)^2}\right] \tag{5}$$

where d_{porous} is the equivalent surface diameter of the porous material expressed as $d_{\text{porous}}=6^{V'_{\text{porous}}}/S'_{\text{porous}}$

Species concentration equation:

$$\varepsilon_{\text{eff}}\left(u\frac{\partial C_k}{\partial x}+v\frac{\partial C_k}{\partial y}+w\frac{\partial C_k}{\partial z}\right) = D_{k,\text{eff}}\left(\frac{\partial^2 C_k}{\partial x^2}+\frac{\partial^2 C_k}{\partial y^2}+\frac{\partial^2 C_k}{\partial z^2}\right)+S_{\text{c}}+S_{\text{L}} \tag{6}$$

Table 1
Source terms in the governing equations

	S_u	S_v	S_w	S_c
Channel	0	0	0	–
GDL	$-\frac{\nu\varepsilon_{\text{eff}}^2}{k_\text{p}}u-\frac{\varepsilon_{\text{eff}}^3 C_\text{F}\rho u}{\sqrt{k_\text{p}}}\sqrt{u^2+v^2+w^2}$	$-\frac{\nu\varepsilon_{\text{eff}}^2}{k_\text{p}}v-\frac{\varepsilon_{\text{eff}}^3 C_\text{F}\rho v}{\sqrt{k_\text{p}}}\sqrt{u^2+v^2+w^2}$	$-\frac{\nu\varepsilon_{\text{eff}}^2}{k_\text{p}}w-\frac{\varepsilon_{\text{eff}}^3 C_\text{F}\rho w}{\sqrt{k_\text{p}}}\sqrt{u^2+v^2+w^2}$	0
Catalyst layer	$-\frac{\nu\varepsilon_{\text{eff}}^2}{k_\text{p}}u-\frac{\varepsilon_{\text{eff}}^3 C_\text{F}\rho u}{\sqrt{k_\text{p}}}\sqrt{u^2+v^2+w^2}$	$-\frac{\nu\varepsilon_{\text{eff}}^2}{k_\text{p}}v-\frac{\varepsilon_{\text{eff}}^3 C_\text{F}\rho v}{\sqrt{k_\text{p}}}\sqrt{u^2+v^2+w^2}$	$-\frac{\nu\varepsilon_{\text{eff}}^2}{k_\text{p}}w-\frac{\varepsilon_{\text{eff}}^3 C_\text{F}\rho w}{\sqrt{k_\text{p}}}\sqrt{u^2+v^2+w^2}$	$\text{H}_2: -\frac{1}{2FC_{\text{total,a}}}\cdot j_\text{a}$; $\text{O}_2: -\frac{1}{4FC_{\text{total,c}}}\cdot j_\text{c}$; $\text{H}_2\text{O}: \frac{1}{2FC_{\text{total,c}}}\cdot j_\text{c}$
Membrane	$-\frac{\nu\varepsilon_{\text{eff}}^2}{k_\text{p}}u-\frac{\varepsilon_{\text{eff}}^3 C_\text{F}\rho u}{\sqrt{k_\text{p}}}\sqrt{u^2+v^2+w^2}+\frac{k_\text{p}}{\nu}Z_\text{f}C_{\text{H}^+}F\cdot\nabla\Phi\cdot u_x$	$-\frac{\nu\varepsilon_{\text{eff}}^2}{k_\text{p}}v-\frac{\varepsilon_{\text{eff}}^3 C_\text{F}\rho v}{\sqrt{k_\text{p}}}\sqrt{u^2+v^2+w^2}+\frac{k_\text{p}}{\nu}Z_\text{f}C_{\text{H}^+}F\cdot\nabla\Phi\cdot v_y$	$-\frac{\nu\varepsilon_{\text{eff}}^2}{k_\text{p}}w-\frac{\varepsilon_{\text{eff}}^3 C_\text{F}\rho w}{\sqrt{k_\text{p}}}\sqrt{u^2+v^2+w^2}+\frac{k_\text{p}}{\nu}Z_\text{f}C_{\text{H}^+}F\cdot\nabla\Phi\cdot w_z$	$\frac{ZF}{RT}D_{k,\text{eff},\text{H}^+}C_{\text{H}^+}\left(\frac{\partial^2\Phi}{\partial x^2}+\frac{\partial^2\Phi}{\partial y^2}+\frac{\partial^2\Phi}{\partial z^2}\right)$

where C_k is the concentration of the kth species and S_c and S_L are the source terms for the chemical reaction and liquid water in the species concentration equation. S_c differs for the various reactant gases, e.g. S_c is $-j_\text{a}/2FC_{\text{total,a}}$ for hydrogen, $-j_\text{c}/4FC_{\text{total,c}}$ for oxygen, and $j_\text{c}/2FC_{\text{total,c}}$ for water vapor. The parameters j_a and j_c, denote the current densities on anode and cathode sides, respectively, which can be calculated using the Butler–Volmer equations [39]:

$$j_\text{a} = Aj_{0,\text{a}}^{\text{ref}}\left(\frac{C_{\text{H}_2}}{C_{\text{H}_2}^{\text{ref}}}\right)\left[\text{e}^{(\alpha_\text{a}F/RT)\eta}-\frac{1}{\text{e}^{(\alpha_\text{c}F/RT)\eta}}\right] \tag{7}$$

$$j_\text{c} = Aj_{0,\text{c}}^{\text{ref}}\left(\frac{C_{\text{O}_2}}{C_{\text{O}_2}^{\text{ref}}}\right)\left[\text{e}^{(\alpha_\text{a}F/RT)\eta}-\frac{1}{\text{e}^{(\alpha_\text{c}F/RT)\eta}}\right] \tag{8}$$

where Aj_0^{ref} is the reference exchange current density, α_a and α_c the electrical charge transport rates in the anode and cathode catalyst layers, η the overpotential, F the Faraday's constant, R the gas constant and T is the temperature of the fuel cell. The local current density distribution was calculated from the phase potential equation:

$$\frac{\partial}{\partial x}\left(\sigma_\text{m}\frac{\partial\Phi}{\partial x}\right)+\frac{\partial}{\partial y}\left(\sigma_\text{m}\frac{\partial\Phi}{\partial y}\right)+\frac{\partial}{\partial z}\left(\sigma_\text{m}\frac{\partial\Phi}{\partial z}\right)=S_j \tag{9}$$

where Φ is the phase potential and σ_m is the membrane conductivity which can be calculated using the formulas developed by Springer et al. [2]:

$$\sigma_\text{m}(T)=\sigma_\text{m}^{\text{ref}}\exp\left[1268\left(\frac{1}{303}-\frac{1}{T}\right)\right] \tag{10}$$

where $\sigma_\text{m}^{\text{ref}}$ is the reference conductivity of the membrane expressed as

$$\sigma_\text{m}^{\text{ref}}=0.005139\lambda-0.00326 \tag{11}$$

$$\lambda=\begin{cases}0.043+17.81a-39.85a^2+36.0a^3, & 0\le a\le 1\\ 14+1.4(a-1), & 1<a\le 3\end{cases} \tag{12}$$

where a denotes the vapor activity and λ the water content in the PEM, S_j in Eq. (9) is the electrical source term, which is zero in the PEM without electrochemical reaction and is $-j_\text{a}$ or $-j_\text{c}$ on the anode or cathode sides. The current density, i, is related to the phase potential Φ as:

$$i_x=-\sigma_\text{m}\frac{\partial\Phi}{\partial x} \tag{13}$$

$$i_y=-\sigma_\text{m}\frac{\partial\Phi}{\partial y} \tag{14}$$

$$i_z=-\sigma_\text{m}\frac{\partial\Phi}{\partial y} \tag{15}$$

Eq. (9) can then be rewritten as

$$\frac{\partial i_x}{\partial x}+\frac{\partial i_y}{\partial y}+\frac{\partial i_z}{\partial z}=S_j \tag{16}$$

The water management strongly affects the of PEMFC performance. In practice, the liquid water in the porous material occupies the pore and, thus, reduces the gas transport in the porous layers. To simplify the complex two-phase flow, the liquid water is assumed to be motionless, with the water only affecting the effective porosity and the mass diffusivity in the gas-diffusion and catalyst layers. When the water vapor partial pressure is greater than the water vapor saturation pressure, the water vapor is assumed to condense and fill the pores in the porous media. The source term, S_L, in the species concentration equation, which is a function of the liquid water fraction, was evaluated as [14]:

$$S_\text{L}=\begin{cases}M_{\text{H}_2\text{O}}k_\text{c}\dfrac{\varepsilon_{\text{eff}}C_{\text{H}_2\text{O}}}{\rho RT}(P_{\text{H}_2\text{O}}-P_{\text{sat}}), & \text{if } P_{\text{H}_2\text{O}}>P_{\text{sat}}\\ k_\text{e}\varepsilon_{\text{eff}}s(P_{\text{sat}}-P_{\text{H}_2\text{O}}), & \text{if } P_{\text{H}_2\text{O}}<P_{\text{sat}}\end{cases} \tag{17}$$

where M is the molecular weight, k_c and k_e the vapor condensation and evaporation rate constants, and P_{sat} is the water vapor saturation pressure, which was calculated using [33–35]

$$P_{\text{sat}}=10^{-2.1794+0.02953T-9.1837\times10^{-5}T^2+1.4454\times10^{-7}T^3} \tag{18}$$

The saturation rate, s, was defined as the ratio of the pore volume occupied by liquid water to the total pore volume in the porous media. The effective porosity of the porous media was then modified to account for the liquid water:

$$\varepsilon_{\text{eff}}=\varepsilon(1-s) \tag{19}$$

Eqs. (1)–(4), (6) and (16) form a complete set of governing equations in the PEMFC. The boundary conditions at the anode flow channels and the cathode flow channels are that: the inlet flow rates are constant, the inlet gas compositions are constant, and the flows are fully developed at the outlets of the anode and cathode flow channels. The solid walls have no slip and zero flux boundary conditions. At the interfaces between the gas channels, the diffusion layers, the catalyst layers, and the PEM, the velocities, mass fractions, momentum fluxes, and mass fluxes are assumed equal. More details were given by Yan et al. [40].

3. Numerical method

Since these equations for this complex convection–diffusion problem cannot be solved analytically, it was solved using the finite-volume method on a collocated cell-centered grid. The general convection–diffusion equation can be expressed in conservative form as:

$$\frac{\partial}{\partial t}(\rho\phi) + \nabla \cdot (\rho\vec{u}\phi - \Xi_\phi \nabla\phi) = S_\phi \tag{20}$$

where t is the time, ϕ the general dependent variable, Ξ_ϕ the exchange coefficient, S_ϕ the source term, $\vec{u}$ the velocity vector, and ρ is the density. When Eq. (20) is integrated over a control volume, the resulting finite-volume equation is:

$$a_P\phi_P = a_E\phi_E + a_W\phi_W + a_N\phi_N + a_S\phi_S + a_H\phi_H + a_L\phi_L + b \tag{21}$$

where ϕ_P is the value of variable ϕ at node P of the control volume, ϕ_E, …, ϕ_L are the values of the variable at nodes in neighboring control volumes, a_P, …, a_L the coefficients in the discretized equations and b is the source terms for the discretized equation for ϕ. The SIMPLE (Semi Implicit Method for Pressure-Linked Equation) algorithm, developed by Patankar [41], was employed to solve the governing equations.

The cell performance was simulated for a small $X \times Y \times Z = 23\,\text{mm} \times 23\,\text{mm} \times 2.845\,\text{mm}$ cell. The cell has 12 channels (6 inlet flow channels and 6 outlet flow channels for the interdigitated flow channel design) and 11 ribs, all 1 mm thick. The diffusion layer is 0.4 mm thick, the catalyst layer is 0.005 mm thick, and the PEM is 0.035 mm thick as shown in Fig. 2. The flow channel and rib widths are defined as L_c and L_r. The anode flow channels are assumed to be in parallel with $L_c = L_r = 1$ mm since the anode flow channel have little effect on cell performance, while the cathode flow channels were elected parallel or interdigitated flow channels. The effect of the cathode flow channel area ratio on cell performance is analyzed for five different ratios of the flow channel width to the rib width. The flow channel area ratio, A_r, is defined as the ratio of the cathode flow channel area to the total reaction area in a cell, $12L_c/(12L_c + 11L_r)$. In this work, A_r is taken as 0.3, 0.4, 0.522, 0.6 and 0.7, where $A_r = 0.522$ denotes that the widths of the flow channels and the ribs are equal (1 mm). The widths of the flow channel and rib for the various flow channel area ratios are listed in Table 2. The base operating conditions for the fuel cell was assumed to be a fuel cell temperature of 323 K,

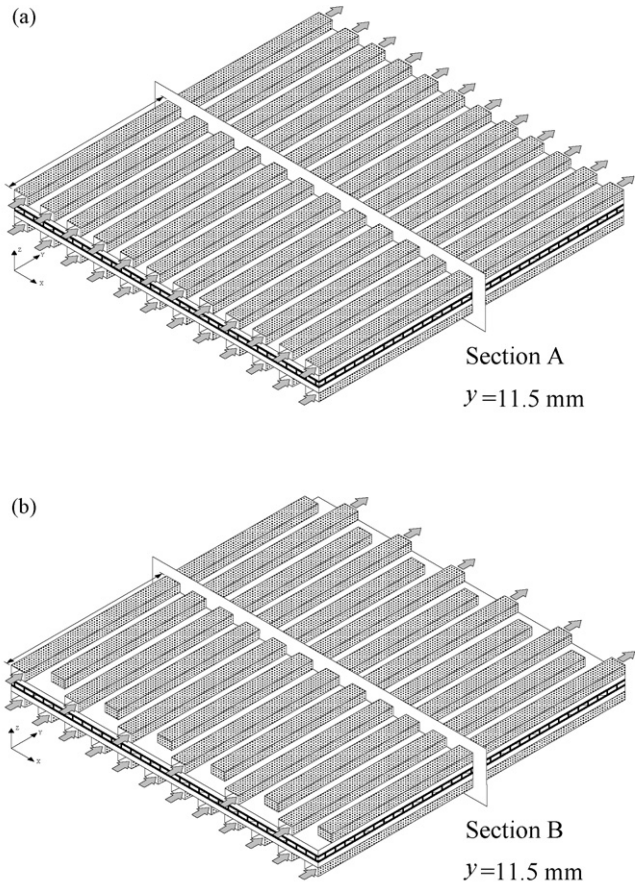

Fig. 2. Schematic diagrams of the PEMFC (a) with the parallel flow channel design and (b) with the interdigitated flow channel design.

the reactant gases on the anode side include hydrogen and water vapor with a relative humidity of 100%, the reactant gases on the cathode side contain oxygen, nitrogen, and water vapor with a relative humidity of 100%, the inlet flow rate on the anode side is 260 $\text{cm}^3\,\text{min}^{-1}$, the inlet flow rate on the cathode side is 700 $\text{cm}^3\,\text{min}^{-1}$, and the inlet pressures on the anode and cathode sides are both 1 atm. All of the fixed parameters used in the model are listed in Table 3. The effects of the cathode flow rate on the cell performance were studied for three other cathode flow rates of 350, 1050 and 1400 $\text{cm}^3\,\text{min}^{-1}$ with the other conditions as same as the base case operating conditions.

The model used non-uniformly distributed elements with 116, 116 and 33 elements in the x, y and z directions, respectively. The grid independence was examined in preliminary test runs. Four non-uniformly distributed grid configurations were evaluated for PEMFC with the parallel flow channel design and

Table 2
The widths of flow channel and rib for the various flow channel area ratio

A_r	L_c (mm)	L_r (mm)
0.3	0.575	1.464
0.4	0.767	1.255
0.522	1.000	1.000
0.6	1.150	0.836
0.7	1.342	0.627

Table 3
Fuel cell parameters

Parameter	Value
$Aj_{0,a}^{ref}$	9×10^8 A m^{-3}
$Aj_{0,c}^{ref}$	1.5×10^2 A m^{-3}
α_a	0.5
α_c	1.5
$\varepsilon_{channel}$	1
$\tau_{channel}$	1
$k_{channel}$	∞ m^2
ε_{GDL}	0.5
τ_{GDL}	1.5
k_{GDL}	1.76×10^{-10} m^2
ε_{CL}	0.4
τ_{CL}	1.5
k_{CL}	1.76×10^{-11} m^2
ε_{Mem}	0.28
τ_{Mem}	Dagan Model
k_{Mem}	1.8×10^{-18} m^2

$A_r = 0.522$. The numbers of elements in the x, y and z directions were: (I) $70 \times 70 \times 25$, (II) $93 \times 93 \times 33$, (III) $116 \times 116 \times 33$, and (IV) $116 \times 116 \times 41$. The influence of number of elements on the polarization curves (I–V curves) for the fuel cell is shown in Fig. 3. The polarization curve for grid (I) differs from those for grids (II–IV). At an operating voltage of 0.3 V, the deviation is about 3.9%. However, the calculated polarization curves for grids (II–IV) do not show any notable differences. At an operating voltage of 0.3 V, the difference between the current densities for (II) and (III) is about 0.32% and the difference for (III) and (IV) is about 0.25%. Grid (III) was chosen for the simulations as a tradeoff between accuracy and execution time. The coupled set of equations was solved iteratively, with the solution considered to be converged when the relative error in each field between two consecutive iterations was less than 10^{-6}. In this work, the CPU time (Intel Core 2 Duo E6300) for each case was about 20 h.

The numerical results were validated by comparing the present predictions with previous experimental results. Fig. 4 compares the calculated polarization curve with experimental data [42] for a fuel cell with the parallel flow channel design and an area of 140 mm × 140 mm. There is only a small difference between the numerical results and the experimental data. Hence, the three-dimensional numerical model can be used to accurately analyze the effects of the flow channel area ratio and cathode fuel flow rate on the cell performance.

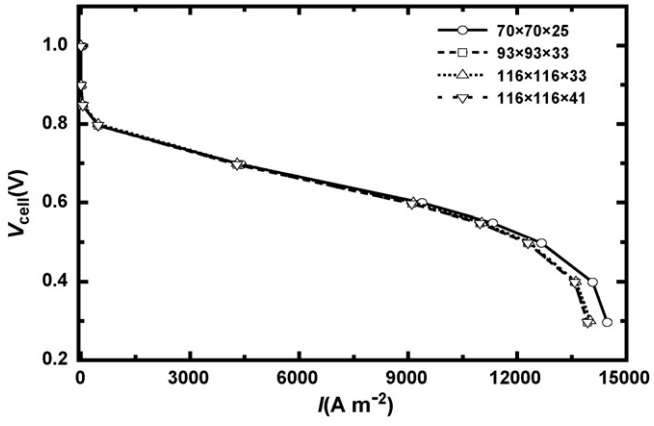

Fig. 3. Influence of the number of elements on the polarization curves.

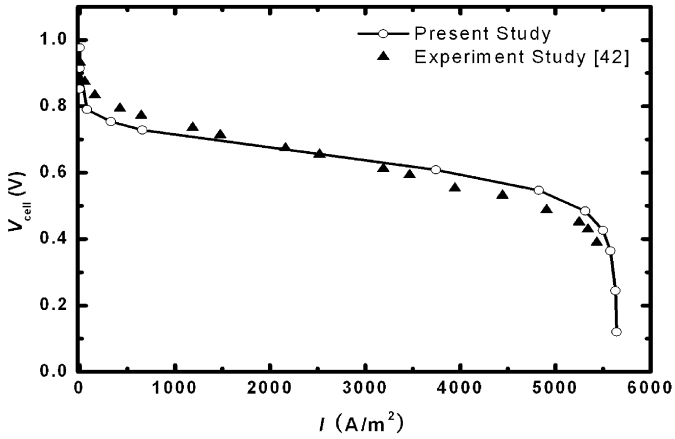

Fig. 4. Comparison of predicted and measured polarization curves for a fuel cell with the parallel flow channel design.

4. Results and discussion

4.1. Effect of flow channel area ratio

The effects of A_r on the I–V_{cell} and I–Power curves are presented in Fig. 5. Compared with the parallel flow channel design, the interdigitated flow channel design increases the limiting current density and considerably improves the cell performance. The fuel transport is mainly by diffusion in the parallel flow channel design, while it is primarily by forced convection in the interdigitated flow channel design. The forced convection greatly increases the oxygen transport rate and ensures that even at low operating voltages enough oxygen is still provided for the catalyst layer to maintain the electrochemical reaction. Forced convection also generates large shear stresses, which efficiently remove the excessive liquid water produced by the electrochemical reaction, which reduces water flooding at the cathode and increases the mass transport in the fuel cell. At operating voltages greater than 0.7 V, the flow channel type and flow channel area ratio have little effect on the cell performance because the electrochemical reaction rate is low and only a limited amount of oxygen is consumed with only a small amount of liquid water produced. Therefore, the oxygen transport rates for both flow channel types and all flow channel area ratios are sufficient to maintain the reaction rates. On the contrary, for low operating voltages, the flow channel design significantly affects the cell performance. For the parallel flow channel design, since the fuel transport into the porous layers is mainly by diffusion, the large flow channel area ratio, which represents a large contact area between the fuel and the diffusion layer, allows more fuel to directly diffuse into the catalyst layer and participate in the electrochemical reaction, resulting in improved cell performance. However, for the interdigitated flow channel design, because the forced convection produced by the baffles efficiently increases

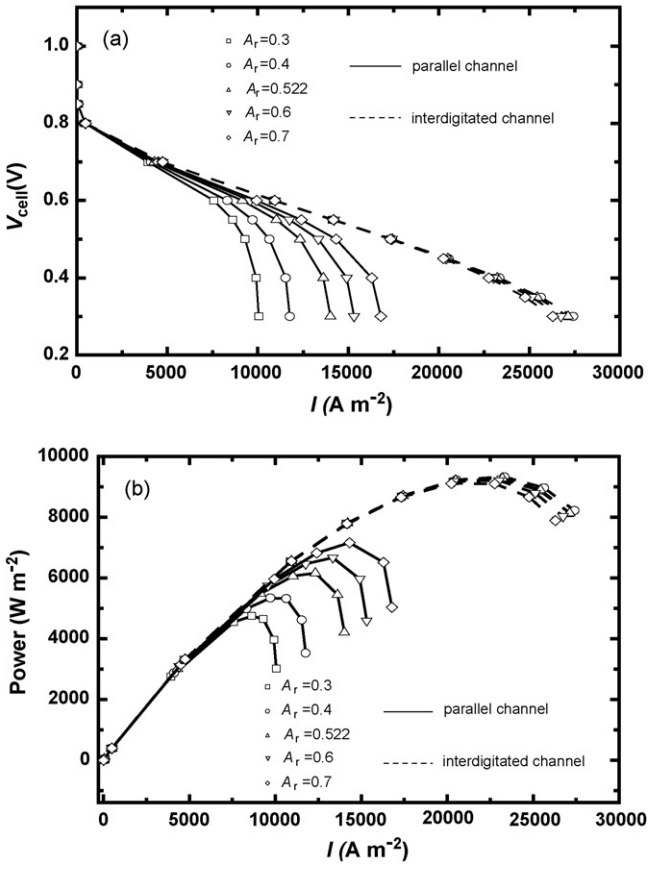

Fig. 5. Effects of the flow channel area ratio on the cell performance. (a) *I–V* curves; (b) *I*–Power curves.

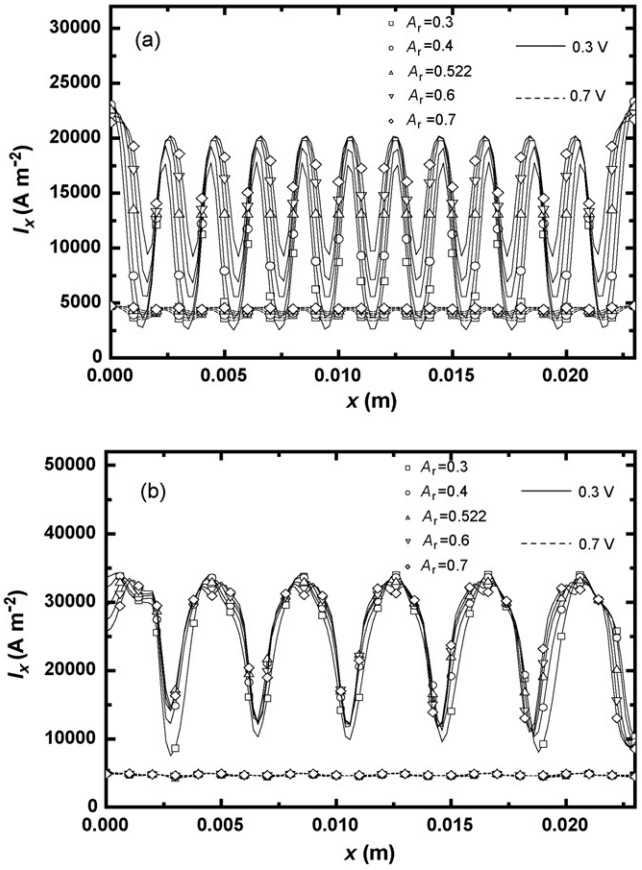

Fig. 6. Effects of the flow channel area ratio on the local current density distribution (y = 11.5 mm). (a) Parallel flow channel design; (b) interdigitated flow channel design.

the fuel transport into the porous layers, the flow channel area ratio is not important and has relatively little effect on cell performance. Fig. 4 shows that the effect of the flow channel area ratio gradually increases for the interdigitated flow channel design as the operating voltage is reduced. For example, at an operating voltage of 0.4 V, the current densities for the five area ratios differ by 560 A m^{-2}, while at 0.3 V, the difference is 1100 A m^{-2}. For the interdigitated flow channel design, the cell with $A_r = 0.7$ has the worst performance while the cell with $A_r = 0.4$ has the best performance.

Fig. 6 shows the current density distribution at $y = 11.5$ mm on the middle cross-section of the PEM at operating voltages 0.3 and 0.7 V for the parallel and interdigitated flow channel designs. At the high operating voltage of 0.7 V, the flow channel type and the flow channel area ratio have almost no impact on the local current densities. The local current densities are all 5000 A m^{-2} under the flow channels and under the ribs for both the parallel flow channel design and the interdigitated flow channel design, far less than at the lower operating voltage. Hence the cell performance is not dependent on the flow channel design at higher operating voltages. At low operating voltages, the flow channel design significantly affects the cell performance. At 0.3 V, the local current densities for the two types of flow channel designs are quite different, while they are quite similar for the various flow channel area ratios for the same flow channel type. The local current densities for the interdigitated flow channel design are much higher than for the parallel flow channel design, indicating that the interdigitated flow channel design significantly improves the cell performance. For the parallel flow channel design, the current densities under the flow channels are larger than under the ribs since the diffusion path for oxygen arriving in the catalyst layer under the ribs is longer than for under the flow channels and the stronger shear stress under the flow channels enhances the liquid water removal. With increasing flow channel area ratio, the local current densities under both the flow channels and the ribs increase for the parallel flow channel design. Therefore, the overall cell performance improves as the flow channel area ratio increases. With the baffles at the ends of the flow channels, the flow channels in the interdigitated flow channel design are divided into inlet flow channels and outlet flow channels, and their local current density distributions differ from those in the parallel flow channel design. The local current density distribution along the x direction shows: the maximum occurs in the inlet flow channel (peaks in Fig. 6b), then decrease under the rib on the right side of the inlet flow channel, which further decrease under the outlet flow channel to the minimum (valleys in Fig. 6b). The current densities then increases again under the rib on the right side of the outlet flow channel to the maximum under the next inlet flow channel. Although the flow channel area ratio has relatively little effect on cell performance for the interdigitated flow channel design, Fig. 6b shows that

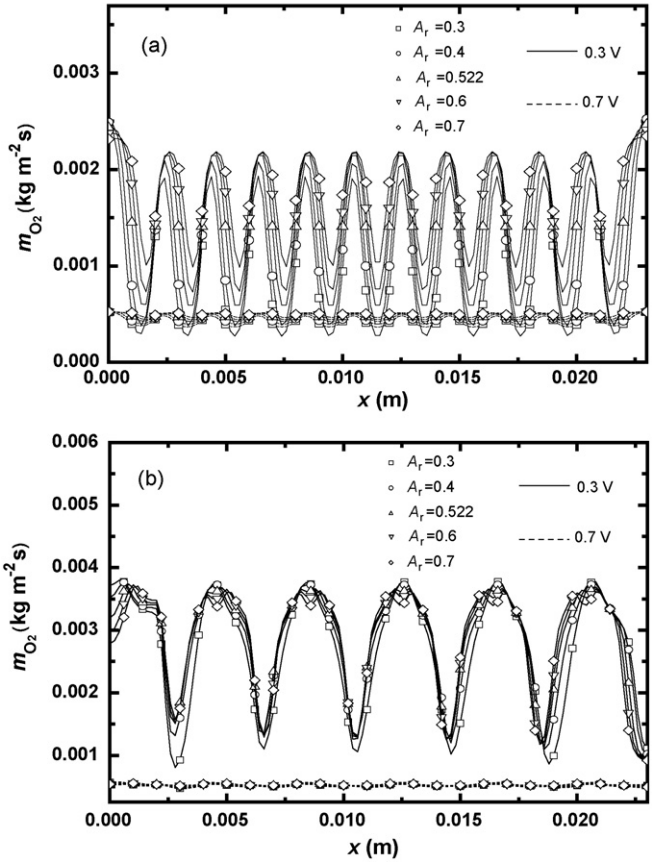

Fig. 7. Effects of the flow channel area ratio on the local oxygen mass flow rate along the interface between the cathode diffusion layer and the catalyst layer (y = 11.5 mm). (a) Parallel flow channel design; (b) interdigitated flow channel design.

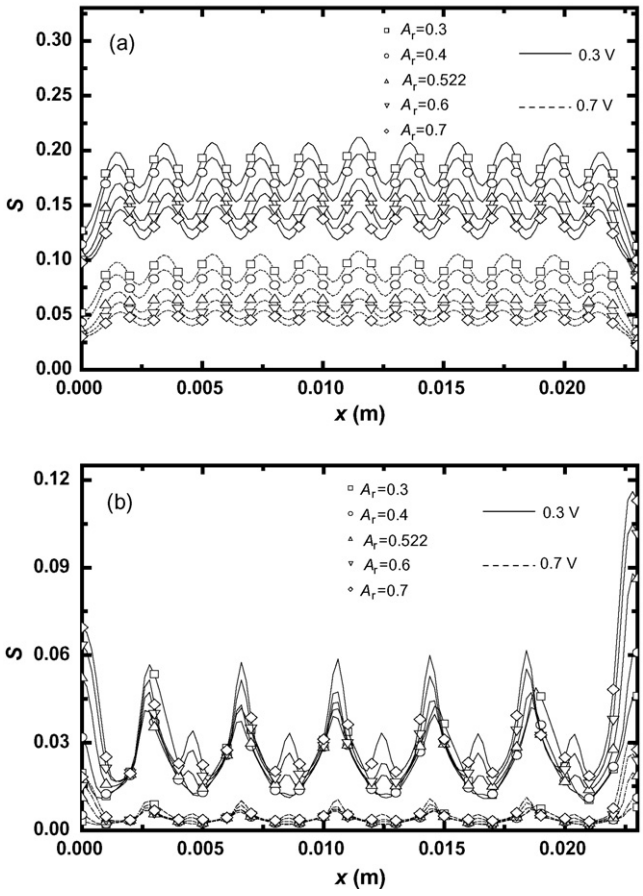

Fig. 8. Effects of the flow channel area ratio on the local liquid water distribution along the interface between the cathode diffusion layer and the catalyst layer (y = 11.5 mm). (a) Parallel flow channel design; (b) interdigitated flow channel design.

the local current densities under the outlet flow channels for the cell with $A_r = 0.4$ are higher than for the cell with $A_r = 0.3$ and are almost equal to the other three flow channel area ratios, and that the local current densities under the inlet flow channels approach the cell with $A_r = 0.3$ and are larger than the other three flow channel area ratios, so $A_r = 0.4$ gives the best performance.

The local oxygen concentrations and liquid water distributions inside the fuel cell directly affect the local current density distribution and the cell performance. Figs. 7 and 8 show the effects of the flow channel area ratio on the local oxygen mass flow rates and liquid water distributions along the interface between the cathode diffusion layer and catalyst layer (at y = 11.5 mm) at operating voltages of 0.3 and 0.7 V for the parallel and interdigitated flow channel designs. At the higher operating voltage of 0.7 V, for both the parallel and interdigitated flow channel designs, the local oxygen mass flow rates and liquid water concentrations for the various flow channel area ratios are all less than at the lower operating voltage of 0.3 V, indicating that the oxygen consumption and the liquid water production rate are both less due to the slower chemical reaction rate at the higher operating voltage. At the lower operating voltage of 0.3 V, both the flow channel type and the flow channel area ratio significantly affect the local oxygen mass flow rates and liquid water distributions along the interface between the cathode diffusion layer and the catalyst layer. The oxygen mass flow rates are lower and the liquid water concentrations are higher for the parallel flow channel design than for the interdigitated flow channel design, so the parallel channel cell performance is worse. For the parallel flow channel design, the oxygen mass flow rates are larger under the flow channels but rapidly decrease under the ribs, while the liquid water concentration displays the opposite trend. As the flow channel area ratio increases, the oxygen mass flow rates increase under both the flow channels and the ribs, while the liquid water concentrations decrease. For the interdigitated flow channel design, the oxygen mass flow rates and liquid water distributions are quite different from the parallel flow channel design, while they are quite similar for the various flow channel area ratios. The oxygen mass flow rate reaches a maximum under the inlet flow channel; gradually decreases under the rib on the right side of the inlet flow channel, and then further decreases to a minimum under the outlet flow channel. The oxygen flow rate then gradually increases again under the next rib to a maximum under the next inlet flow channel. The liquid water distributions are lowest under the inlet flow channel, increase under the rib on the right side of the inlet flow channel, and continue to increase under the neighboring outlet flow channel to a maximum. The liquid water distributions then

decrease under the neighboring rib to a minimum under the next inlet flow channel.

Comparison of Figs. 6–8 indicates that the local current density distributions are dependent on the local oxygen mass flow rates and liquid water distributions. The high oxygen mass flow rates along the interface between the cathode diffusion layer and the catalyst layer means that more oxygen diffuses into the catalyst layer to participate in the electrochemical reaction and more liquid water is generated, resulting in a higher local current density. For the parallel flow channel design, since the fuel enters the porous layers mainly by diffusion, as the flow channel area ratio increases, the contact area between the oxygen and the diffusion layer increases so more oxygen directly diffuse into the porous layers and participates in the electrochemical reaction, so the cell performance is improved. For the interdigitated flow channel design, the fuel is forced to enter the diffusion layer at the end of the inlet flow channel due to the baffles, thus the fuel utilization efficiency is increased. Meanwhile, the higher stresses produced by the forced convention help remove the liquid water. Therefore, the cell performance of the interdigitated flow channel design is higher than that of the parallel flow channel design. Although more liquid water is produced by the electrochemical reaction in the diffusion and catalyst layers under the flow channels, high shear forces carry the liquid water to under the adjacent ribs and the outlet flow channels, thus providing higher oxygen mass flow rates in the diffusion and catalyst layers under the flow channels. Under the ribs and the outlet flow channels, the oxygen mass flow rates are lower and the electrochemical reaction is weaker with less liquid water production. However, the liquid water from under the inlet flow channels is carried there, so a large amount of liquid water accumulates under outlet flow channels. Excessive liquid water in the porous layers blocks the porous media pores and reduces the oxygen transport and the electrochemical reaction rates. Therefore, at lower operating voltages, the liquid water distribution strongly affects the oxygen transport rates and the local current density distributions, which ultimately affect cell performance.

Fig. 9 shows the effect of the flow channel area ratio on the cathode pressure drop in the cells with the parallel and interdigitated flow channel designs. Fig. 8 indicates that the cell pressure losses are almost independent of the operating voltages, but depend strongly on the flow channel area ratio. As the flow channel area ratio increases, the cell pressure losses decrease. Since the cathode oxygen flow rates are the same in the present simulations, the larger flow channel area ratios result in lower fuel inlet velocities and fuel flow resistance. The pressure losses in the interdigitated flow channel design are two to three times the losses in the parallel flow channel design.

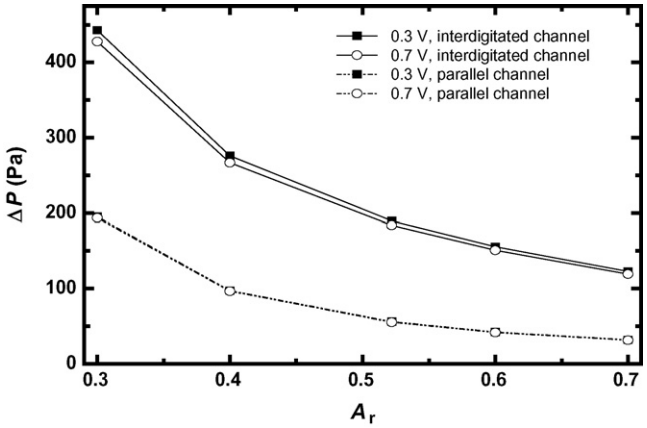

Fig. 9. Effects of the flow channel area ratio on the pressure losses at the cathode.

4.2. Effects of cathode fuel flow rate

The anode reactant gas into the fuel cell is assumed to be humidified hydrogen, while the cathode reactant gas is humidified air; thus, the most economic means is to change the cathode air flow rates for improving cell performance. The effect of the cathode flow rate on cell performance was also investigated for the parallel and interdigitated flow channel designs with various flow channel area ratios. Besides the base case flow rate of 700 $cm^3\ min^{-1}$, the cathode flow rates also were taken as 350, 1050, and 1400 $cm^3\ min^{-1}$ with the other operating conditions the same as for base case flow rate. Fig. 10 shows the effects of the cathode flow rate and flow channel area ratio on the average current densities of cells with parallel and interdigitated flow channel designs at operating voltages of 0.3 and 0.7 V. At the higher operating voltage, the average current densities for the

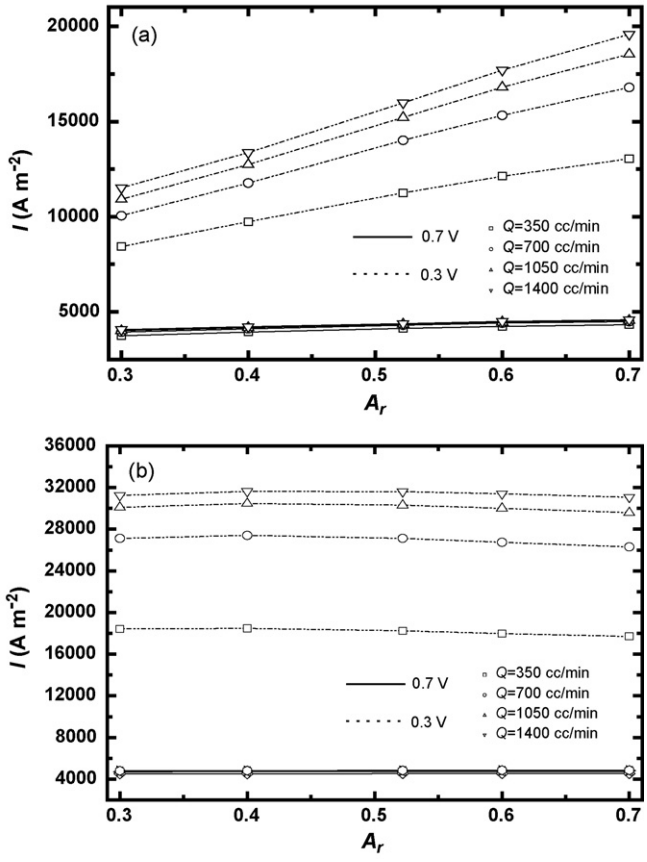

Fig. 10. Effects of the flow channel area ratio and cathode flow rates on the average current densities. (a) Parallel flow channel design; (b) interdigitated flow channel design.

Table 4
The average current densities for the various flow channel area ratios at the operating voltage of 0.3 V

Q (cm^3 min^{-1})	I (A m^{-2})				
	$A_r = 0.3$	$A_r = 0.4$	$A_r = 0.522$	$A_r = 0.6$	$A_r = 0.7$
350	18,441	18,469	18,241	17,987	17,711
700	27,124	27,407	27,132	26,747	26,296
1050	30,093	30,461	30,317	29,996	29,589
1400	31,246	31,636	31,606	31,399	31,080

various cathode flow rates, various flow channel types and various flow channel area ratios are almost the same, indicating that the flow channel design and operating conditions do not affect the cell performance. At the lower operating voltage of 0.3 V, the cathode flow rates significant impact the cell performance. With increasing cathode flow rates, the average current densities increase and the cell performance improves, but the rate of increase gradually weakens, because increasing cathode flow rates means increasing oxygen inlet velocities, thus more oxygen is provided to the catalyst layer for the electrochemical reaction and higher oxygen velocities also help remove liquid water. For the parallel flow channel design, the cell performance improves with increasing flow channel area ratios for all cathode flow rates, while for the interdigitated flow channel design, the cell performance first increases then decreases with increasing flow channel area ratios for all cathode flow rates, indicating that there is an optimal flow channel area ratio. The average current densities at the operating voltage of 0.3 V for the interdigitated flow channel design are listed in Table 4. Apparently, for the given operating conditions, the best cell performance occurs for a flow channel area ratio of $A_r = 0.4$ and the worst occurs for the flow channel area ratio of $A_r = 0.7$ for all cathode flow rates.

The local current density, oxygen concentration and liquid water distributions inside the cell are analyzed for $A_r = 0.4$ and 0.7 to further understand the effects of the cathode flow rate and the flow channel area ratio on cell performance. At higher operating voltages, the flow channel design and operating conditions have little effect on the cell performance; therefore, the following analysis will focus on the lower voltage of 0.3 V. Fig. 11 shows the current density distribution at $y = 11.5$ mm in the middle cross-section of the PEM for the parallel and interdigitated flow channel designs at various cathode flow rates. The local current density distributions at the various cathode flow rates are similar to those at 700 cm^3 min^{-1}, but with the peaks and valleys of the local current densities all increasing with increasing cathode flow rates. Therefore, the average current densities increase and overall cell performance improves. For the interdigitated flow channel design, the local current density valleys for $A_r = 0.7$ are slightly higher than for $A_r = 0.4$, while the local current densities under the flow channels (whose peaks should occur) have a local valley as seen in Fig. 11, so that current density peaks for $A_r = 0.7$ are much lower than for $A_r = 0.4$. Because the current densities at the peaks of about 30,000 A m^{-2} make a larger contribution to the average current density, the average current density for $A_r = 0.7$ is lower than for $A_r = 0.4$ and its cell performance is worse.

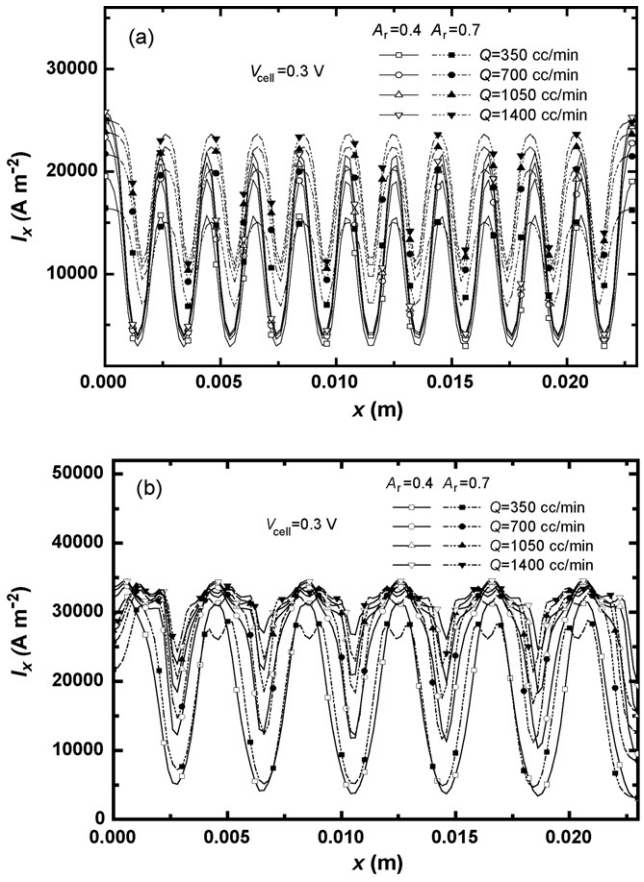

Fig. 11. Effects of the flow channel area ratio and cathode flow rate on the local current density distribution ($y = 11.5$ mm). (a) Parallel flow channel design; (b) interdigitated flow channel design.

Figs. 12 and 13 show the local oxygen flow rates and the liquid water concentrations at $y = 11.5$ mm along interface between the cathode diffusion layer and the catalyst layer for the parallel and interdigitated flow channel designs. Comparison of Figs. 12 and 13 show that the local current density distributions are very consistent with the local oxygen flow rates and they all increase with increasing cathode flow rates. The larger oxygen flow rates along the interface between the diffusion layer and the catalyst layer mean that more oxygen enters the catalyst layer to participate in electrochemical reaction; thus, the reaction rates are higher and the current densities are larger. The local liquid water concentrations are just the opposite. As the cathode flow rates increase, the liquid water concentration decreases; thus, the ratio of the pore volume occupied by liquid water to the total pore volume in the porous layers decreases and oxygen transport rate increases, so more oxygen is transported into the catalyst layer and the current densities rise. The high electrochemical reaction rates produce more liquid water, but because the high cathode flow rates more efficiently remove the liquid water, the liquid water concentrations are lower. For the parallel flow channel design, at the same cathode flow rate, the liquid water concentrations along the interface between the diffusion layer and the catalyst layer decrease with increasing flow channel area ratio, while for the interdigitated flow channel design, at the same cathode flow rate, the liquid concentrations for $A_r = 0.7$

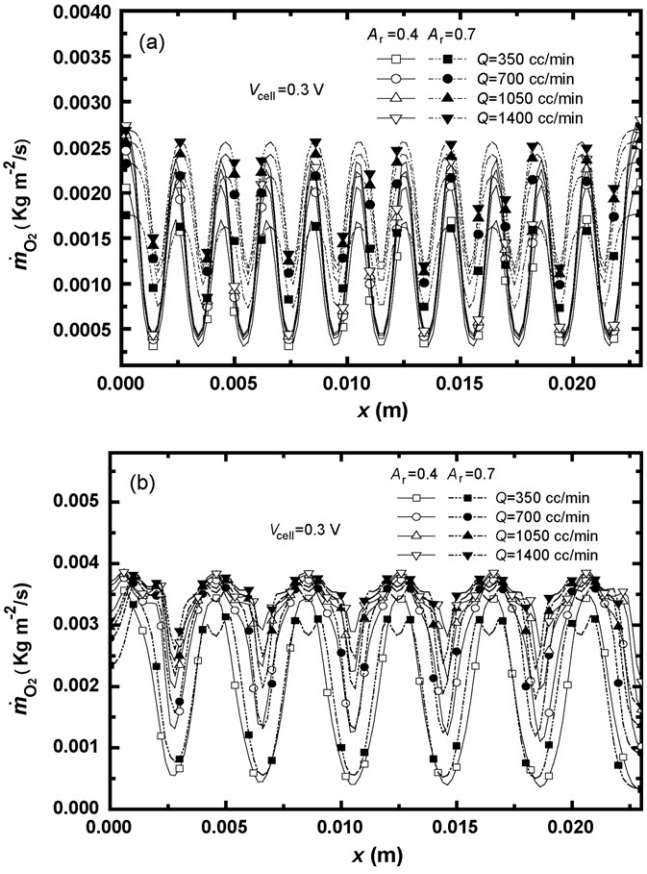

Fig. 12. Effects of the flow channel area ratio and cathode flow rate on the local oxygen mass flow rate along the interface between the cathode diffusion layer and the catalyst layer (y = 11.5 mm). (a) Parallel flow channel design; (b) interdigitated flow channel design.

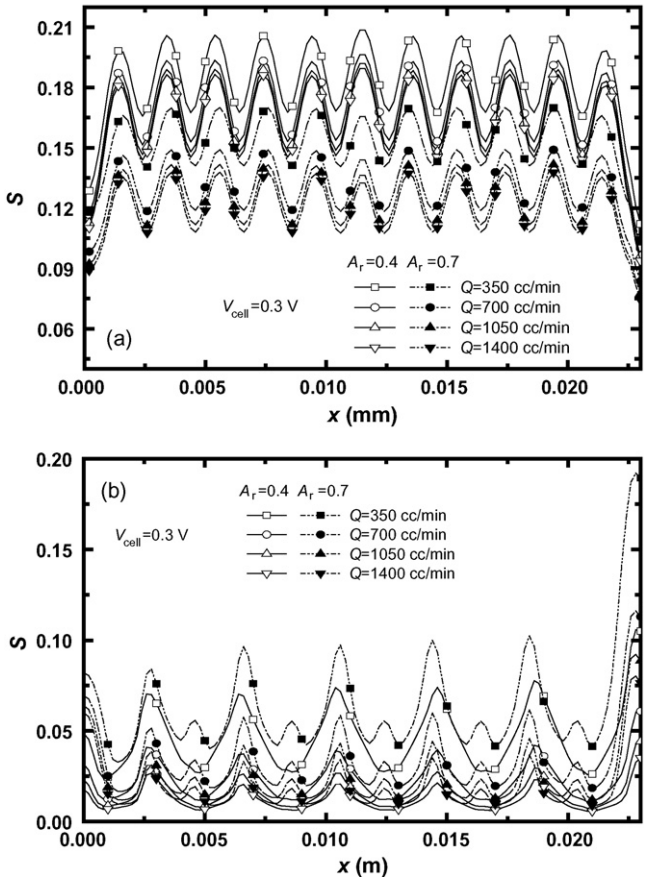

Fig. 13. Effects of the flow channel area ratio and cathode flow rate on the local liquid water distribution along the interface between the cathode diffusion layer and the catalyst layer (y = 11.5 mm). (a) Parallel flow channel design; (b) interdigitated flow channel design.

are larger than for $A_r = 0.4$. Especially under inlet the flow channels, the liquid water concentrations for $A_r = 0.7$ exhibit local peaks within the valleys, which increases the oxygen transport resistance and reduces the local current densities. As a result, decreases occur in the current densities at their peaks in Fig. 11 for $A_r = 0.7$. Thus, the overall cell performance for $A_r = 0.7$ is worse than for $A_r = 0.4$. This analysis further indicates that an appropriate flow channel design is an efficient means to improve cell performance, by not only enhancing the liquid water removal but also increasing the oxygen transport rates. Other operating parameters, such as increasing the cathode flow rate, also improve the cell performance.

Fig. 14 shows the cell pressure losses for the parallel and interdigitated flow channel designs with $A_r = 0.4$ and 0.7 for various cathode flow rates. The pressure losses for the interdigitated flow channel design are higher than for the parallel flow channel design due to the baffles. Fig. 14 shows that for the same flow channel area ratio of $A_r = 0.4$, the pressure losses in the interdigitated flow channel design are about 50% higher than in the parallel flow channel design. For $A_r = 0.7$, the pressure losses in the interdigitated flow channel design are about twice the losses in the parallel flow channel design. The cell pressure losses also increase as the cathode flow rate increases or the flow channel area ratio decreases.

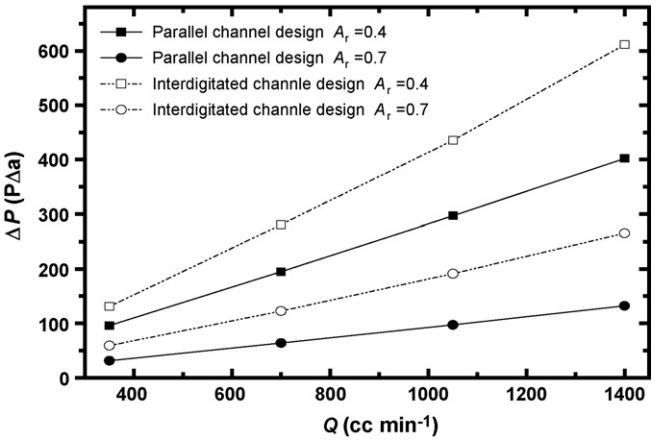

Fig. 14. Effects of the flow channel area ratio and cathode flow rate on the pressure losses at the fuel cell cathode.

5. Conclusions

Appropriate flow channel design is an effective means for improving cell performance. The present paper presented a three-dimensional transport model based on the finite-volume method to analyze the effects of the flow channel area ratio

and cathode flow rate on the cell performance and local transport characteristics of PEMFC with parallel or interdigitated flow channel designs. At higher operating voltages, the cell performance is independent of the flow channel design and the operating parameters, while at lower operating voltages, both significantly affect cell performance. For the parallel flow channel design, the fuel is transported into the diffusion layer and catalyst layer mainly by diffusion; thus, as the flow channel area ratio increases the cell performance improves, because the larger flow channel area ratio increases the contact area between the fuel and the diffusion layer, which allows more fuel to directly diffuse into the porous layers to participate in the electrochemical reaction and enhance the reaction rates. For the interdigitated flow channel design, the baffles force the fuel into the porous layers to increase participation in the electrochemical reaction; thus, the flow channel area ratio has little effect on cell performance. The forced convection not only increases the fuel transport rates but also enhances the liquid water removal, both of which increase cell performance compared with the parallel flow channel design. The optimal performance for the interdigitated flow channel design occurs for a flow channel area ratio of 0.4. The cell performance also improves as the cathode flow rates increase.

Acknowledgment

This study was supported by the National Natural Science Foundation of China (No. 50636020)

References

[1] D.N. Bernadi, M.W. Verbrugge, AIChE J. 37 (8) (1991) 1151–1163.
[2] T.E. Springer, T.A. Zawodizinski, S. Gottesfeld, J. Electrochem. Soc. 138 (1991) 2334–2342.
[3] V. Gurau, F. Barbir, H. Liu, J. Electrochem. Soc. 47 (2000) 2468–2477.
[4] N. Djilali, D. Lu, Int. J. Therm. Sci. 41 (2002) 29–40.
[5] T.F. Fuller, J. Newman, J. Electrochem. Soc. 140 (5) (1993) 1218–1225.
[6] H.V. Bussel, F. Koene, R. Mallant, J. Power Sources 71 (1998) 218–222.
[7] D. Singh, D.M. Lu, N. Djilali, Int. J. Eng. Sci. 37 (1999) 431–452.
[8] J.S. Yi, T.V. Nguyen, J. Electrochem. Soc. 145 (4) (1998) 1149–1159.
[9] J.S. Yi, T.V. Nguyen, J. Electrochem. Soc. 146 (1999) 38–45.
[10] I.M. Hsing, P. Futerko, Chem. Eng. Sci. 55 (2000) 4209–4218.
[11] S.H. Ge, B.L. Yi, J. Power Sources 124 (2003) 1–11.
[12] W.M. Yan, C.Y. Soong, F. Chen, H.S. Chu, J. Power Sources 125 (2004) 27–39.
[13] S. Dutta, S. Shimpalee, J.W. Van Zee, J. Heat Mass Transfer 44 (2001) 2029–2042.
[14] S. Mazumder, J.V. Cole, J. Electrochem. Soc. 150 (2003) A1503–] A1509.
[15] S. Mazumder, J.V. Cole, J. Electrochem. Soc. 150 (2003) A1510–A1517.
[16] S. Um, C.Y. Wang, Three-dimensional analysis of transport and reaction in proton exchange membrane fuel cells, in: The 2000 ASME International Mechanical Engineering Congress & Exposition, Walt DisneyWorld Dolphin, Orlando, FL, USA, November 5–10, 2000.
[17] S. Um, C.Y. Wang, J. Power Sources 125 (2004) 40–51.
[18] T.V. Nguyen, R.E. White, J. Electrochem. Soc. 140 (1993) 2178–2186.
[19] H.H. Voss, D.P. Wilkimson, P.G. Pickup, M.C. Johnson, V. Basura, Electrochim. Acta 40 (1995) 321–328.
[20] T. Okada, X. Gang, M. Meeg, Electrochim. Acta 43 (14-15) (1998) 2141–2155.
[21] T. Okada, G. Xie, O. Gorseth, S. Kjelstrup, N. Nakamura, T. Arimura, Electrochim. Acta 43 (1998) 3741–3747.
[22] D.L. Wood, J.S. Yi, V. Nguyen, Electrochim. Acta 43 (24) (1998) 3795–3809.
[23] J.J. Baschuk, X. Li, J. Power Sources 86 (2000) 181–196.
[24] T.V. Nguyen, J. Electrochem. Soc. 143 (5) (1996) L103–L105.
[25] A.C. West, T.F. Fuller, J. Appl. Electrochem. 6 (1996) 557–565.
[26] A. Kazim, H.T. Liu, P. Forges, J. Appl. Electrochem. 29 (1999) 1409–1416.
[27] M. Hu, A. Gu, M. Wang, X. Zhu, L. Yu, Energy Convers. Manage. 45 (2004) 1861–1882.
[28] M. Hu, A. Gu, M. Wang, X. Zhu, L. Yu, Energy Convers. Manage. 45 (2004) 1883–1916.
[29] W. He, J.S. Yi, T.V. Nguyen, AIChE J. 46 (10) (2000) 2053–2064.
[30] F. Chen, Y.G. Su, C.Y. Soong, W.M. Yan, H.S. Chu, J. Electroanal. Chem. 566 (2004) 85–93.
[31] C.Y. Soong, W.M. Yan, C.Y. Tseng, H.C. Liu, F. Chen, J. Power Sources 143 (2005) 36–47.
[32] W.M. Yan, C.Y. Soong, F. Chen, H.S. Chu, J. Power Sources 143 (2005) 48–56.
[33] H.C. Liu, W.M. Yan, C.Y. Soong, F. Chen, J. Power Sources 142 (2005) 125–133.
[34] J.H. Jang, W.M. Yan, H.Y. Li, Y.C. Chou, J. Power Sources 159 (2006) 468–477.
[35] H.C. Liu, W.M. Yan, C.Y. Soong, F. Chen, H.S. Chu, J. Power Sources 158 (2006) 78–87.
[36] W.M. Yan, C.H. Yang, C.Y. Soong, F. Chen, M.C. Mei, J. Power Sources 160 (2006) 284–292.
[37] W.M. Yan, C.Y. Chen, S.C. Mei, C.Y. Soong, F. Chen, J. Power Sources 162 (2006) 1157–1164.
[38] F.A.L. Dullien, Porous Media, Academic Press, New York, 1991.
[39] V. Gurau, H. Liu, S. Kakac, AIChE J. 44 (1998) 2410–2422.
[40] W.M. Yan, H.C. Liu, C.Y. Soong, F. Chen, C.H. Cheng, J. Power Sources 161 (2006) 907–919.
[41] S.V. Patankar, Numerical Heat Transfer and Fluid Flow, Hemisphere/McGraw-Hill, New York, 1980.
[42] C.H. Cheng, Development of shape designer for the flow channels of bipolar plate for PEM fuel cells (2/3), Technical Report of NSC-93-2212-E-036-001, National Science Council, Taiwan, 2004.